Published in final edited form as:
Neuroscience. 2013 October 22; 251: 75–89. doi:10.1016/j.neuroscience.2012.04.061.

Beyond counts and shapes: Studying pathology of dendritic spines in the context of the surrounding neuropil through serial section electron microscopy

Masaaki Kuwajima[1], **Josef Spacek**[2], and **Kristen M. Harris**[1,3,*]

[1]Center for Learning and Memory, The University of Texas at Austin

[2]Charles University Prague, Faculty of Medicine in Hradec Kralove, Czech Republic

[3]Section of Neurobiology, The University of Texas at Austin

Abstract

Because dendritic spines are the sites of excitatory synapses, pathological changes in spine morphology should be considered as part of pathological changes in neuronal circuitry in the forms of synaptic connections and connectivity strength. In the past, spine pathology has usually been measured by changes in their number or shape. A more complete understanding of spine pathology requires visualization at the nanometer level to analyze how the changes in number and size affect their presynaptic partners and associated astrocytic processes, as well as organelles and other intracellular structures. Currently, serial section electron microscopy (ssEM) offers the best approach to address this issue because of its ability to image the volume of brain tissue at the nanometer resolution. Renewed interest in ssEM has led to recent technological advances in imaging techniques and improvements in computational tools indispensable for three-dimensional analyses of brain tissue volumes. Here we consider the small but growing literature that has used ssEM analysis to unravel ultrastructural changes in neuropil including dendritic spines. These findings have implications in altered synaptic connectivity and cell biological processes involved in neuropathology, and serve as anatomical substrates for understanding changes in network activity that may underlie clinical symptoms.

Keywords

3D reconstruction; connectome; neuropil; pathology; scanning transmission electron microscopy; ultrastructure

*Corresponding author: Dr. Kristen M. Harris (kharris@mail.clm.utexas.edu; 1 University Station, C7000, Austin, TX 78712, U.S.A.; tel 1-512-232-3968) .

1. Why use serial section electron microscopy to study dendritic spines and related structures in pathology?

1.1. Diversity of the dendritic spine structure

Ever since they were described by Ramón y Cajal in 1888 (Ramón y Cajal, 1995), dendritic spines have been identified as the main sites of excitatory synaptic contacts in brain areas that contain spiny neurons. In the normal brain, dendritic spines exhibit a wide variety of sizes and shapes, ranging from a simple spine with a bulbous head attached to a narrow neck emanating from the dendrite, to a thorny excrescence with multiple heads and synapses. Spine dimensions vary in volume, surface area, length, neck diameter, and head diameter. For example, the volume of two neighboring spines on the same dendritic segment can vary by more than an order of magnitude (Fiala et al., 2002). During the period of synaptogenesis, long (> 2 μm) highly motile protrusions called filopodia emerge from dendrites and axons. These filopodia are filled with a densely-stained matrix of actin cytoskeleton and often form multiple nascent synapses along their lengths (Dailey and Smith, 1996; Fiala et al., 1998). As the synaptic connections become more mature, dendrites start to show more mature spines that typically form just one excitatory synapse with one presynaptic bouton (Fiala et al., 1998). The formation of mature spines with single synapses may result from retraction of filopodia, loss of synapses with boutons that were outcompeted, or emergence of spines from shaft synapses (Fiala et al., 1998). Occasionally, a single presynaptic bouton forms synapses with multiple postsynaptic structures, which can be either spines or dendritic shafts (Shepherd and Harris, 1998; Sorra and Harris, 1993). Actin cytoskeleton supports dynamic regulation of spine shapes (Frost et al., 2010). At the ultrastructural level, a variety of organelles and other subcellular structures are observed within dendritic spines, including smooth or coated vesicles and tubules, multi-vesicular bodies, smooth endoplasmic reticulum (which can become a highly elaborated structure called the spine apparatus in large spines), and polyribosomes (Spacek and Harris, 1997; Cooney et al., 2002; Bourne and Harris, 2011a). Excitatory synapses on spines are identified by the postsynaptic density (PSD), which is an electron-dense thickening adjacent to the postsynaptic membrane that is composed of many scaffolding and signaling molecules (Sheng and Hoogenraad, 2007; Harris and Weinberg, 2012). PSD size scales with the size of spine and presynaptic bouton (Harris and Stevens, 1988; Harris and Stevens, 1989; Harris and Sultan, 1995), and large excitatory synapses have perforated or segmented PSDs (Peters and Kaiserman-Abramof, 1969; Spacek, 1985; Lisman and Harris, 1993). Molecular and cell biological processes involved in brain pathology may affect any of these characteristics of dendritic spines. Morphological abnormalities of spines may underlie altered synaptic connectivity and network activity, which in turn manifest as clinical symptoms, in many disorders discussed in this special issue (Glausier and Lewis., 2012; He and Portera-Calliau, 2012; Hof et al., 2012; Leuner and Shors, 2012; Licznerski and Duman, 2012; Nithianantharajah and Hannan, 2012; Pozueta et al., 2012; Villalba and Smith, 2012; Wong and Guo, 2012) and elsewhere (e.g., Penzes et al., 2011; Russo et al., 2010).

1.2. Multiple facets of dendritic spine pathology: distribution, morphology, subcellular structures, and synaptic connections

In our previous review on dendritic spine pathology (Fiala et al., 2002), we classified pathological changes according to two general categories. The first category included pathologies of spine synapse distribution, resulting in changes in the density of spines along the length of the dendritic shaft and changes in spine gross morphology. Commonly observed morphological changes include altered spine size or shape, formation of varicosities along dendritic shafts with concomitant loss of spines, and spine formation in abnormal locations. Virtually all light microscopic studies attempt to measure these characteristics of gross dendritic and spine morphology, while overlooking the other

category of spine pathology: pathologies of ultrastructure. These include characteristics that can only be revealed at electron microscopic resolutions, and include, for example, electron-opaque cytoplasm, hypertrophy of organelles or spine volumes, and the formation of spines without presynaptic boutons.

Because dendritic spines are sites of synaptic contacts, pathology of dendritic spines likely represents only a partial picture of a larger pathology in neuronal connectivity and circuitry. There is a tight correlation between the size of PSD and the composition of vesicles in presynaptic boutons (Harris and Stevens, 1988; Harris and Stevens, 1989; Harris and Sultan, 1995), as well as the amount of coverage by perisynaptic astroglial processes (Witcher et al., 2007). Thus, changes (pathological or otherwise) observed in postsynaptic spines likely involve concomitant remodeling in presynaptic boutons and perisynaptic astrocytes, and vice versa. Also, there are presynaptic and glial factors that affect spine morphology (e.g., Henkemeyer et al., 2003; Garcia et al., 2010), which lead us to believe that spine pathology is unlikely to be purely a postsynaptic phenomenon. Therefore, studying dendritic spine pathology should be considered as part of a larger effort to understand pathological changes in neural circuitry that underlie clinical symptoms of various disorders.

With advances in molecular genetics and fluorescent microscopy techniques, the last decade has seen an explosion of knowledge regarding the genetic and molecular mechanisms that regulate spine morphology and functions under a wide variety of conditions, including synaptic plasticity and models of brain disorders (many of which are reviewed in this special issue; Glausier and Lewis., 2012; He and Portera-Calliau, 2012; Hof et al., 2012; Leuner and Shors, 2012; Licznerski and Duman, 2012; Nithianantharajah and Hannan, 2012; Pozueta et al., 2012; Villalba and Smith, 2012; Wong and Guo, 2012). These studies typically use metrics of gross spine morphology (e.g., protrusion counts, shapes, and volume) at the light microscopic level, typically visualized with Golgi-impregnation or fluorescent molecules. Then the changes in spine morphology are used as readouts of experimental manipulations, aided by molecular, genetic, and/or pharmacological techniques. These studies are often carried out in preparations that allow for direct access for such manipulations and observation of neurons, namely cultured primary neurons and slice tissue. Connectivity and functional states of these spines or spine-like protrusions can greatly vary in experimental systems, depending on many factors including the methods of preparation and the age of the cells/tissue. Cultured rat hippocampal neurons (at 21 days *in vitro* with astrocyte feeding layer) exhibit about five spines per 10 μm of dendritic length, and about half of the synapses are on the dendritic shaft (Boyer et al., 1998). CA1 apical dendrites in organotypic slice culture exhibit about 10 spines per 10 μm of dendrite (Mateos et al., 2007). In comparison, oblique dendrites of perfusion-fixed adult rat hippocampal CA1 neurons can have 30-40 spines per 10μm of dendritic length, and synapses on dendritic shafts are rare (e.g., Harris and Kater, 1994; Bourne et al., 2007). Both *in vitro* experimental systems are useful for unraveling molecular signaling mechanisms for regulation of spine morphology, and electrophysiological methods can be used with relative ease of tissue access to assess synapse functions and circuitry activity. However, it is often difficult to know how results from these systems can be extrapolated to connectivity and functions of neuronal circuitry *in vivo*. Organotypic slices retain at least some of the local circuitry as well as glial cells but lack the full complement of extrinsic and intrinsic connections. Neurons and their circuitries extend over large volumes, so better understanding of neuronal circuitry would require the ability to image neuropil over large volumes.

1.3. Technical difficulties in imaging larger brain tissue volumes

The Golgi-impregnation technique has traditionally been used to visualize dendritic spines in intact brain tissues from animal models and postmortem human brains, as well as brain biopsies (e.g., Purpura, 1974; Graveland et al., 1985). Although this approach in the human

tissue has played an important role in laying the foundation of our understanding regarding spine morphology under pathological conditions, it is very difficult to identify and count individual dendritic spines unequivocally when they are overlapping with each other or extending in or out of the imaging plane. Recent developments utilizing *in vivo* imaging techniques with two-photon laser scanning microscopy has allowed for direct visualization of fluorescent-labeled spines in the intact living brains of animals *in vivo*. In combination with functional imaging using Ca^{2+}-sensitive fluorescent dye and/or transgenic animals expressing fluorescent protein in a small subset of neurons, it is now possible to study the structure of dendritic spines in the context of local circuit activity (Knott and Holtmaat, 2008; Holtmaat and Svoboda, 2009). Still, this approach is limited to observing the superficial layers of the neocortex, and it remains a major challenge to image tissue deeper in the brain at a resolution high enough to capture fine details of neuropil elements that are densely packed. The signal-to-noise ratio is low when imaging fluorescence in small structures like spines *in vivo*, and the intrinsic properties of the tissue itself (i.e., refraction index is not homogeneous throughout the tissue) degrade imaging resolution. Perhaps "super-resolution" microscopy methods, such as stimulated emission depletion microscopy and stochastic optical reconstruction microscopy (Huang et al., 2009; also see Mancuso et al., 2012, in this issue), could improve the accuracy of such spine measurements, but these techniques are not yet capable of imaging multiple colors and dynamic *in vivo* processes deep in brain tissue. Although these fluorescence-based methods allow for highly selective labeling (and therefore are useful for tracking a molecule of interest in a cell, or for molecular profiling of neuropil elements like spines), it is easy to overlook the cellular context in these studies where > 95% of the neighboring tissue is *not* visualized. Serial section electron microscopy (ssEM) can visualize all spines, synapses, axons, and subcellular structures, which allows key questions to be addressed, such as: "How are 'pathological' spines different from normal ones in connectivity with axonal boutons in the surrounding neuropil?"

Transmission electron microscopy (TEM) was used in the 1950's to confirm that dendritic spines are indeed the sites of excitatory synaptic contacts in brain areas containing spiny neurons (Palay and Palade, 1955; Gray, 1959). Since then, serial thin sections of < 100 nm thickness have been used to visualize them in the three-dimensional (3D) context of the surrounding neuropil, including dendrites, axons, and astroglial process (e.g., Thaemert, 1966; Novikoff et al., 1971; Spacek and Lieberman, 1974). Recently, ssEM has gained renewed interest in neuroscience as a high-resolution 3D tool (Stevens et al., 1980). It has been used for 3D reconstruction of functionally identified local circuitry (Bock et al., 2011; Briggman et al., 2011), as well as for attempts to map all synaptic connections in the brain (termed "connectome") (Helmstaedter et al., 2008; Mishchenko et al., 2010; Anderson et al., 2011a). Our laboratory and others use ssEM to understand how the structure of synapses and neuropil is modified by experience (or in models of learning and memory; e.g., Ostroff et al., 2002; Knott et al., 2006; Bourne and Harris, 2011a) or in pathological conditions (Spacek, 1987; Fiala et al., 2007; Nuntagij et al., 2009; Witcher et al., 2010; Hara et al., 2011; Popov et al., 2011; Villalba and Smith, 2011). Such modifications of synaptic structures can ultimately alter the connection profile for a neuron, providing the necessary anatomical foundation for changes in information processing and behavioral output. The pathological disruption in spine morphology may involve critically subcellular structures (e.g., polyribosomes, microtubules, endosomes, dense core vesicles, and smooth endoplasmic reticulum), which are reliably identified and analyzed from ssEM images with a pixel size of ≤ 2 nm.

2. Technical considerations for ssEM

In order to take advantage of advanced ssEM tools for studying synapse structures in pathological conditions, one must start with well-preserved brain tissue. We have previously described our routine methods to generate series of high-quality serial EM images from neuropil in the hippocampal formation of acute slice and perfusion-fixed brain tissue embedded in epoxy resin (Harris et al., 2006; Kuwajima et al., 2012; also see http://synapses.clm.utexas.edu/). Here, we briefly outline our tissue processing protocols and discuss factors that affect ultrastructural preservation and quality of serial sections (also see Bourne and Harris, 2011b).

2.1. Tissue processing

Because ssEM requires that the specimens be fixed, it can only provide "snapshots" of the dynamic changes in normal spine morphology (Matus, 2000; Blanpied and Ehlers, 2004). Thus, it is critical to control carefully for factors such as the stage of a disease, age of patient/subject, sex, as well as period in the reproductive cycle. The animals can be naïve, or those that underwent behavioral studies and other experimental manipulations including *in vivo* functional imaging. The combination of ssEM and *in vivo* functional imaging in particular offers a great opportunity to study ultrastructure of synapses in relation to functionally identified local circuitry (Bock et al., 2011; Briggman et al., 2011).

When using model animals, excellent ultrastructural preservation can be achieved by rapid perfusion-fixation with mixed aldehydes while the animal is under artificial ventilation to avoid hypoxic damages (Tao-Cheng et al., 2007). In our protocol for perfusion-fixation of adult rats (Kuwajima et al., 2012), an anesthetized animal is placed under artificial respiration so that the brain tissue does not become hypoxic until the perfusate is delivered at pressure higher than physiological blood pressure (up to 180 mmHg). An air pump is used to apply the constant pressure because pumps of other types (e.g., peristaltic) often cause pulsatile delivery of the perfusate at too slow a rate. The blood is first washed off from the system by several seconds of perfusion with oxygenated buffer solution maintained at body temperature. This buffer is at physiological pH and osmolality to keep the tissue from undergoing confounding structural changes. Spine morphology is sensitive to temperature changes (Kirov et al., 2004; Roelandse and Matus, 2004; Bourne et al., 2007), and tissue swelling or shrinkage can result if the buffer solution is hypotonic or hypertonic (Hayat, 1981). The buffer wash is followed by fixative containing a mixture of formaldehyde and glutaraldehyde in cacodylate buffer. Phosphate buffer is commonly used to prepare fixative for perfusion-fixation, but it can produce electron-opaque particulate artifacts (Hayat, 1981). Artificial ventilation is not performed for mice or juvenile rats due to their small size. In these cases, time between cutting the diaphragm (i.e., loss of breathing) and perfusion with fixative must be as short as possible (30 sec or less) to minimize hypoxic damage to the brain tissue (Tao-Cheng et al., 2007).

Model animals (especially transgenic mice) have served as invaluable tools for establishing causal relationship between risk factors (e.g., genetic mutations and toxins) and specific disease phenotypes. However, they likely represent only some aspects of the human diseases because of the heterogeneity in underlying risk genes and their complex interactions with environmental factors. Thus, pathological observations in human patients should set the context for the knowledge gained from the animal models, which in turn could serve as references for better understanding human neuropathology. For ssEM analysis of neuropil in the human brain tissue, specimens can be obtained during the course of neurosurgery in patients suffering from tumors (Spacek, 1987) or pharmacoresistant epilepsy (Witcher et al., 2010). Despite caveats regarding human brain studies, such as individual medical history and symptom heterogeneity, these are the best sources of information regarding various

aspects of human brain architecture at the ultrastructural level, which would not be possible to determine otherwise.

Traditionally, human brain specimens have been chemically fixed by immersion immediately after resectioning (Alonso-Nanclares et al., 2008). However, artifacts may develop due to hypoxia during this process because it may take minutes between surgical resectioning and immersion in the fixative. Alternatively, the tissue can retain excellent ultrastructure if it is recovered in artificial cerebrospinal fluid in an interface chamber for several hours (Fiala et al., 2003) before being fixed rapidly with aldehydes facilitated by microwave irradiation (Witcher et al., 2010). This microwave-enhanced chemical fixation can be applied successfully to acute slice preparations from experimental animals as well (Bourne et al., 2007). Although rapid freezing methods (such as high-pressure freezing) have been used to produce excellent ultrastructure and retain tissue antigenicity (Studer et al., 2008; McDonald, 2009), these methods have not been used widely for ssEM studies because the tissue with high-quality preservation is often limited to very small volumes located unpredictably throughout the region of interest. Even so, ssEM of brain tissue from rapid freezing offers the possibility of using post-embedding immunogold labeling to study ultrastructural localization of proteins in relation to neuropil in the 3D context (see Section 3.2; Nuntagij et al., 2009).

Once the tissue is fixed well, it is sectioned to the thickness of ≤ 100 μm in order to achieve rapid and uniform penetration of osmium tetroxide. The tissue then undergoes microwave-enhanced *en bloc* staining with heavy metals and dehydration, followed by embedding into epoxy resin (Feinberg et al., 2001). Then, serial thin sections of uniform thickness must be obtained from a precisely targeted brain region of interest. The use of the “Chien mold” (Figs. 1A-C) facilitates precise targeting of area of interest, especially in layered structures such as the hippocampal formation, neocortex, and cerebellar cortex, because it allows the tissue to be cut from two perpendicular planes. Using a diamond trim tool (e.g., DiATOME cryotrim 20) allows precise shaping of the final block face (gray shaded area in Fig. 1C) for serial sectioning, and a 35° knife causes less tissue compression compared to a 45° one (Harris et al., 2006). We typically cut 200-300 serial sections at a 45 nm thickness setting on the ultramicrotome (e.g., Leica UC7) from a target location, while minimizing flaws, such as folds, knife marks, and debris from stain or dust (Fig. 1D; Harris et al., 2006; Kuwajima et al., 2012). There is no particular limit to the number of serial sections that can be obtained and imaged other than the skill of the operator and time. The thickness of 45 nm was chosen to minimize overlaps of small organelles within individual ultrathin sections (e.g., small synaptic vesicles are ~30 nm in diameter), facilitating more accurate identification and counting of those small subcellular structures. Real section thickness, however, must be estimated later to calibrate a serial section series during image analysis, because the actual thickness almost always shows slight variations from the nominal section thickness (i.e., the feed setting on the ultramicrotome). We use the cylindrical mitochondria method to calculate the ratio of the maximum diameter of longitudinally sectioned mitochondria (or other cylindrical objects) to the number of serial sections they span (Fiala and Harris, 2001a). The section thickness can also be estimated directly with a color 3D laser confocal microscope (Kubota et al., 2009).

2.2. Serial EM imaging techniques

Renewed interest in ssEM in the last decade has led to substantial and ongoing improvements in this otherwise time- and labor-intensive approach. Such improvements include increased image field size, finer z-resolution (i.e., section thickness), reduction or elimination of section loss, reduction of physical and optical distortion, and automation of serial sectioning, imaging, alignment, and segmentation (Briggman and Denk, 2006). In order to implement the appropriate serial EM imaging system to address a particular set of

scientific questions, one must consider the features that ultimately determine the system's limitations. These include (but are not limited to): serial sectioning method (e.g., diamond knife vs. focused ion beam), specimen presentation (e.g., block face vs. ultrathin sections), platform (e.g., scanning vs. transmission EM), imaging mode (e.g., detection of transmitted vs. back-scattered electrons), and imaging field size. The readers are referred to recent review papers detailing these serial EM imaging systems (Helmstaedter et al., 2008; Kleinfeld et al., 2011).

We recently developed a new method for imaging serial ultrathin sections using scanning transmission electron microscopy (STEM) based on a field emission SEM fitted with a multi-mode transmitted electron detector (Fig. 1E; Mendenhall et al., 2009; Kuwajima et al., 2012). This system is capable of semi-automated acquisition of large-field images (single field dimension = 64 μm × 64 μm, or larger with mosaic) at a high resolution (1 or 2 nm pixel size) from multiple grids spanning an entire series of ≥ 200 serial sections loaded on a single specimen holder. With multiple holders, the total section number is only limited by how many have been prepared. Images acquired on this system have less optical distortion and specimen drift, and the resolution is comparable to those taken on a conventional TEM at a magnification of about 5000× with a bottom-mount CCD camera (pixel dimension = 4080 × 4080). Archived serial sections on conventional TEM grids can be imaged on this SEM system without modification, thereby leaving the possibility for post-embedding immunolabeling and EM tomography, which can generate virtual sections of less than 3 nm thickness to investigate small structures in detail (Chen et al., 2008). In addition, less operator involvement is required, and the instrument can be obtained for about half the cost of a conventional TEM with a large-format CCD camera.

Serial sections collected on traditional TEM grids can also be imaged with a TEM custom-fitted with an array of CCD cameras (TEMCA), which rapidly acquires images with larger field size (Bock et al., 2011). However, TEMCA is cumbersome and expensive, and the resulting images can still suffer from the specimen drifting, optical distortion, and beam damage that are inherent in TEM imaging. In other approaches, serial ultrathin sections are collected automatically on electron-opaque plastic tapes (automatic tape-collecting lathe ultramicrotome, or ATLUM; Hayworth et al., 2006) or manually on glass microscope slides (array tomography; Micheva and Smith, 2007) that can be archived for repeated SEM and light microscopy imaging. Array tomography offers a relatively straightforward platform for immunolabeling (which can be repeated for multiple epitopes) and correlative fluorescence and electron microscopy.

Two recently developed serial section EM systems are based on scanning electron microscopy (SEM) with the detection of back-scattered electrons from the block face that is serially removed either by focused ion beam (FIB-SEM; Cantoni et al., 2010; Knott et al., 2011) or diamond knife inside the SEM chamber (SBFSEM; Denk and Horstmann, 2004). These approaches can generate thinner sections (~25 nm for SBFSEM and ~5 nm for FIB-SEM) than the sections obtained for traditional serial EM (~45 nm). Thus, the voxels obtained through FIB-SEM imaging can be more isotropic (several nanometers per side). The FIB-SEM is limited by the size of the field that can be milled and imaged, usually less than 100 μm × 100 μm, while this is not the case with SBFSEM. These methods represent a significant improvement in z-resolution, ease of serial image alignment, elimination of section loss, and reduction of physical and optical distortion. However, the destructive nature of SBFSEM and FIB-SEM precludes post-embedding immunolabeling, re-examination of areas of interest at a higher magnification, or use of EM tomography.

2.3. Analysis of ssEM material

Serial EM images are aligned and analyzed with the aid of computational tools. Our laboratory primarily uses the RECONSTRUCT™ software (Fiala, 2005), which allows for computer-aided manual alignment of serial section images, as well as segmentation, 3D reconstruction, and quantitative measurements of the objects of interest. Ongoing improvements in computational tools are making these steps increasingly automated (as discussed below), but trained human eyes are still necessary for accurate analysis of the serial EM images (Mishchenko et al., 2010).

2.3.1. Dissector stereology—Single-section analysis and two-section dissector stereology traditionally dominated the field of ultrastructural analysis, but the experimental findings can be confounded by missed and incorrectly identified elements, as well as misrepresentation of their dimensions and composition. Many fine neuropil elements are not identifiable on single sections, and size differences can lead to biases. Larger objects are more likely to be counted because they would exhibit enough defining features, but less likely to be identified accurately because a single section is not enough to show all aspects of a large structure. For instance, a large mushroom spine head can appear on a single section as a small head with a short segment of its postsynaptic density (PSD). Thus, quantitative data on dimensions of dendritic spines identified on single sections should be considered as controversial until ssEM-based analyses are used. Stereological analysis is affected by yet another factor: neuropil is not a uniform mesh of dendrites, axons, and glial processes. Thus, the presence of large structures such as blood vessels and soma of interneurons and glia in a relatively small image field can greatly skew counting and density measurements (Harris, 1994). As an alternative, one can extend the two-section dissector stereology to count elements of interest in a volume of tissue from a relatively shorter set of serial section series, just long enough for unequivocal identification of the objects of interest to allow for accurate identification and counting (e.g., many spines and synaptic structures can span dozens of ultrathin sections) (Fiala and Harris, 2001b; Witcher et al., 2010).

2.3.2. Dense vs. sparse reconstruction—The neuropil in a given volume can be reconstructed completely (dense reconstruction) or partially (sparse reconstruction). Dense reconstruction is the most accurate method to quantify connectivity, size, and composition of dendritic spines, synapses, and other associated structures. However, this approach is currently labor-intensive and time-consuming (Mishchenko et al., 2010; Kleinfeld et al., 2011). Much of the current efforts in the field have been devoted to the development and improvement of computational tools for easier handling of stacks of large-field serial images (which can be on the order of teravoxels) for automatic alignment and segmentation, as well as to generate realistic three-dimensional reconstructions of segmented objects (e.g., Fiala, 2005; Chklovskii et al., 2010; Jain et al., 2010; Saalfeld et al., 2010; Anderson et al., 2011b; Helmstaedter et al., 2011; Knowles-Barley et al., 2011; Lang et al., 2011; Morales et al., 2011). Until dense reconstruction can be implemented more routinely through the help of these computational tools, sparse reconstruction serves as the best alternative for quantitative and qualitative evaluation of morphological changes associated with neuropathology, provided that comparable populations of structures are evaluated across conditions. This requires well-defined sets of criteria for sampling, including 1) accurate targeting of brain areas of interest, from which serial section images are acquired, 2) similarity in dendrite caliber and/or branch order, and 3) length and number of dendritic segments to analyze. For our laboratory, accurate targeting of the region of interest involves measuring the distance from the cell body layers in the hippocampal formation so that all sampled areas have the same afferent populations (Fig. 1C). Then we choose dendrites that contain a similar number of microtubules, which is used as an indicator of the dendritic caliber, their capacity for intracellular transport, and availability of synaptic resources (e.g.,

polyribosomes and other organelles) (Fiala et al., 1998; Harris et al., 2007). Finally, we typically reconstruct and analyze dendritic segments spanning about 10 μm so that a wide variety of spines, synapses, and organelles are included in each dendritic segment. We also analyze axonal boutons that form synapses along these dendritic segments, as well as astroglial processes associated with each synapse, thereby revealing a more complete picture of synapse structure and connectivity changes in the 3D context of neuropil. Obviously, these sampling criteria must be determined for each brain area because the architecture of cells and neuropils, and connectivity rules might vary greatly from one brain area to another (DeFelipe, 2010; Lichtman and Denk, 2011).

3. Examples of recent studies employing ssEM to analyze pathological changes in neuropil, including dendritic spines

Here we discuss six recent ssEM studies (Fiala et al., 2007; Nuntagij et al., 2009; Witcher et al., 2010; Hara et al., 2011; Popov et al., 2011; Villalba and Smith, 2011) to demonstrate the use of this method in 3D analysis of highly complex neuropil structures and subcellular organelles in pathological conditions and natural aging. Two of them also feature the implementation of ssEM in combination with immunolabeling techniques to identify specific afferents (Villalba and Smith, 2011) or to localize molecules otherwise invisible (Nuntagij et al., 2009).

3.1. Progressive pathology of synapses and astroglia in the hippocampus of mesial temporal lobe epilepsy patients (Witcher et al., 2010)

Mesial temporal lobe epilepsy (MTLE) is one of the most prevalent and most resistant to pharmacotherapy among various forms of epilepsy that affects about 50 million people world-wide (Spencer, 2002). Seizures are associated with loss of neurons and dendritic spines, as well as varicose dendritic shafts and abnormal morphology of spines and PSD/synapses (Swann et al., 2000). In this study, ssEM was used to examine pathological changes in structure of synapses and astroglia in the human hippocampal tissue that was obtained during surgical treatment of MTLE from patients, ranging from mild to severe stages of histological pathology in the hippocampus. All had intractable MTLE that was alleviated by this treatment. To facilitate ultrastructural preservation, the surgically resected hippocampal tissue was recovered in artificial cerebrospinal fluid before processing for ssEM. Unbiased volume analysis, which allowed for complete identification and measurements of many neuropil elements (Fiala and Harris, 2001b), revealed progressive loss of synapses with pathological severity. The tissue from the severe case exhibited huge extracellular space, and almost all (23 out of 24) synapses were located on just seven multi-synaptic dendritic spines (Figs. 2A and A'). These spines had volumes about 15% larger than normal mushroom spines (in rats), but individual PSDs were smaller than those found on normal mushroom spines. Thus, this pathological spine may have resulted from competition among axons for synaptic sites on the few remaining spines. Multi-synaptic spines were rarely seen in the mild and moderate cases. Astroglial processes also exhibited progressive pathological morphology. Although they appeared normal in the mild case, astroglial processes in the moderate case showed some of the thin processes containing bundles of intermediate filaments. In the severe case thin processes (0.25-0.35 μm diameter) of astrocytes were filled with filaments that were so densely stained that the cytoplasm was completely obscured. Junctional specializations were also found between glial processes in the moderate but not in the mild case, suggesting an increased coupling among astrocytes with disease progression. The volume fraction occupied by astroglial processes was increased in tissues from the moderate and severe cases, while the association of these processes was greatly reduced at the axon-spine interface in the severe case. Overall, synapses with perisynaptic astroglia were larger than those without. In mild and moderate

cases, PSD size was positively correlated with astroglia-free length (i.e., part of axon-spine interface not covered by astroglia), thereby providing larger open routes for spillover of substances, such as glutamate, between larger synapses. Neighboring synapses on a single giant spine in the severe case were contiguous and did not have astroglial processes separating them (Fig. 2B).

The relationship between synapses and astroglial processes has a direct implication in how much glutamate spillover can occur to drive aberrant excitatory neurotransmission, and is particularly important for understanding the pathophysiological mechanisms of epilepsy. Analysis of the synapse-glia relationship requires ssEM because the structure of fine astroglial processes is not resolved at the level of light microscopy, and their continuity and spatial relationship in the neuropil cannot be fully ascertained from single-section EM studies. This study also demonstrates that ssEM can be effectively used in human brain tissue to establish correlations between pathological changes in neuropil structures and disease severity. This type of information is essential not only in better understanding of disease progression in patients, but also in identifying timing and targets of therapeutic interventions.

3.2. Close spatial relationship between amyloid deposits and dendrosomatic plasma membranes (Nuntagij et al., 2009)

Alzheimer's disease (AD), a progressive neurodegenerative disease, is the most common form of dementia. Characteristic pathological features of AD include amyloid plaques, neurofibrillary tangles, and cell death. With a typical onset age of 65, symptoms of AD include progressive loss of memory, critical reasoning and other cognitive functions (Penzes et al., 2011). Cognitive decline in AD has a strong correlation with loss of synapses and dendrites (DeKosky and Scheff, 1990). Naturally secreted oligomers of amyloid β (Aβ) protein disrupt synaptic functions and spine morphology at the light microscopic level (Lacor et al., 2007; Shankar et al., 2007), but it remains unclear how Aβ deposits are distributed in the extracellular space and interact with neuropil in early stages of plaque formation. Nuntagij et al. (2009) addressed this issue by combining ssEM with post-embedding immunogold labeling to identify unequivocally the small deposits of Aβ in relation to the complex neuropil in naturally aging dogs (with mild cognitive deficit) and a transgenic mouse model of AD, carrying mutations in amyloid precursor protein (Swe), tau (P301L), and Presenilin-1 (M146V) (Oddo et al., 2003). The dorsolateral prefrontal cortex of the dogs and the hippocampus of the mice (28-30 months of age) from perfusion-fixed brain underwent rapid freezing, followed by low-temperature substitution and embedding for post-embedding immunogold labeling of Aβ in serial sections (80-160 sections). In both animal models, 3D reconstructions revealed the Aβ deposits shaped in branched and intertwined threads, which can be traced back to an area with particularly high labeling density (Fig. 2C). The deposits were in close proximity to the soma, primary apical dendrites, and large caliber branches, and often found wrapping around these structures (Fig. 2C). In contrast, no association was seen between the Aβ deposits and smaller caliber dendrites, dendritic spines, synapses, or astroglial processes. These observations suggest that plaque formation follows the interaction of secreted Aβ molecule with specific membrane domains in the soma and proximal dendrites, rather than simple polymerization of Aβ in the extracellular space, and raise questions regarding what plasma membrane factors might mediate such interactions. This study did not specifically examine the dendritic spines, but given the apparent lack of direct interactions between spines and Aβ deposits it would be of great interest to see how Aβ oligomers affect spine functions and morphology *in vivo*.

3.3. Mitochondrial degeneration in dystrophic neurites in senile plaque (Fiala et al., 2007)

In addition to the oligomerization of secreted Aβ peptide, plaque formation may also result from degeneration of dystrophic axons (Kimura et al., 2003; Martin et al., 1991). Fiala et al. (2007) used ssEM to examine dystrophic neurites in late stage plaques in the layer 2/3 of prefrontal cortex of very old monkeys (32 years; equivalent to 90-100 years old in humans). Three-dimensional reconstruction and analysis showed that swollen neurites, originating from otherwise normal-appearing neurites, form “diverticula”. Microtubules entered the diverticula from the connecting neurites and formed loops, which effectively trapped mitochondria and other organelles (Fig. 2D). Most of these neurites were traced back to unmyelinated small axons, but their origins were not always clear. The trapped mitochondria exhibited morphological features consistent with degeneration and macroautophagy (e.g., swollen crista and clusters of lamellar bodies; Fig. 2D). A few areas of the plaque contained degenerating neurites and organelles embedded in electron-dense filamentous materials in the extracellular space. These observations appear to be consistent with the idea that intraneuronal aggregation of Aβ (Gouras et al., 2000; D’Andrea et al., 2001; Kimura et al., 2005; Ohyagi, 2008) may result in the disruption of intracellular transport and abnormal accumulation of mitochondria, leading to compromised mitochondrial function and autophagic degeneration. Serial section EM was necessary to identify these complex structures, such as dystrophic neurites containing abnormal arrangements of subcellular structures.

3.4. Reduced connectivity associated with aging and menopause due to changes in synapse size and presynaptic bouton structure in the monkey dentate gyrus (Hara et al., 2011)

Memory impairment commonly occurs in natural aging and during the menopausal transition. In a parallel study, Hara et al. (2012) showed that rhesus monkeys display age- and menopause-related recognition memory impairment, as measured by the hippocampus-dependent delayed nonmatching-to-sample (DNMS) task. In this task, the animal is presented with an object followed by a delay period during which the object is hidden. Then the same object is presented along with a novel one, and the animal is rewarded for choosing the novel. The memory impairment was correlated with reduced density of perforated synapses in the outer molecular layer of the dentate gyrus, but total density of axospinous synapses remained unchanged in all age and menses groups (Hara et al., 2012).

Here, Hara et al. (2011) used ssEM to examine whether age- or menopause-related memory deficits were correlated with changes in the structure of presynaptic boutons in the outer molecular layer of the hippocampal dentate gyrus. Vesicle-filled presynaptic boutons usually form a single synapse (single-synaptic bouton), but they occasionally form synapses with multiple postsynaptic targets (multi-synaptic bouton, or MSB; Fig. 2E) or have no postsynaptic partner at all (non-synaptic bouton, or NSB). Aged female monkeys had a significantly higher proportion of NSBs and concomitantly lower proportion of MSBs, which also had a lower number of synaptic contacts on average. These changes were correlated with deficits in DNMS performance (such as average accuracy and number of trials to criterion). Although proportions of different bouton types were similar across menses groups, peri- and post-menopausal monkeys had fewer MSBs contacting perforated synapses with segmented PSDs (Fig. 2E), which also correlated with DNMS performance deficits. These results suggest that age- and menopause-related changes in a subset of synaptic connectivity in the dentate outer molecular layer may be associated with deficits in recognition memory. Connectivity changes due to multi- or non-synaptic boutons could only be detected by ssEM analysis (also see Villalba and Smith [2011] below).

3.5. Reduced connectivity at the mossy fiber-CA3 synapses in a mouse model of Down syndrome due to structural changes in postsynaptic thorny excrescences (Popov et al., 2010)

Down's syndrome (DS) is the most common genetic cause of mental retardation, results from trisomy of chromosome 21, and occurs in about 1 out of 1000 live births (Roizen and Patterson, 2003). The Ts65Dn mouse model of DS is based on trisomy of the distal segment of the mouse chromosome 16, which is homologous to the long arm of the human chromosome 21 (Davisson et al., 1993). These mice exhibit cognitive impairment analogous to symptoms seen in DS patients, such as deficits in hippocampus-dependent spatial learning (Reeves et al., 1995; Demas et al., 1996; Hyde et al., 2001). In order to elucidate anatomical substrates underlying these deficits, Popov et al. (2010) used a combination of ssEM and stereological methods to study the morphological characteristics of spines and synapses in the hippocampal dentate gyrus (middle molecular layer) and thorny excrescences in the area CA3 (Fig. 2F). Volume stereological counting showed a reduction in the number of asymmetric synapses on spines and dendritic shafts in the dentate middle molecular layer of Ts65Dn mice, consistent with previous observations (Kurt et al., 2004). Random sampling of 3D reconstructed mushroom spines from the middle molecular layer revealed that a smaller proportion of these spines contained multi-vesicular bodies, which are part of the endosomal system (Huotari and Helenius, 2011). Interestingly, ssEM analysis of the CA3 thorny excrescences revealed a reduced number of thorns per excrescence, as well as accompanying reduction in the volume of individual thorns and the number of spinules per thorn. Interestingly, there was no significant change in the volume of mossy fiber boutons synapsing on these excrescences, although their vesicle contents were not analyzed. Together with a previous neurophysiological study indicating a reduced frequency of mossy fiber-mediated miniature excitatory postsynaptic currents in the CA3 of cultured hippocampal slices from Ts65Dn mice (Hanson et al., 2007), this observation suggests a decrease in functional inputs from the dentate granule cells to CA3 pyramidal neurons. Serial section EM analysis was essential in detecting changes in the distribution of multi-vesicular bodies, as well as the structure of the highly complex neuropil elements like the thorny excrescences.

3.6. Afferent-specific remodeling of synapses and organelles in a non-human primate model of Parkinson's disease (Villalba and Smith, 2011)

Medium spiny neurons (MSNs) of the striatum (Caudate and Putamen in primates) receive dopaminergic afferents from the substantia nigra pars compacta, and major glutamatergic afferents from the neocortex and the thalamus (both forming axospinous synapses) (Smith et al., 1998; Smith et al., 2009). The GABAergic MSNs in turn project to the external globus pallidus (striatopallidal) or the substantia nigra pars reticulata (striatonigral). A major pathological feature of Parkinson's disease is the loss of the nigrostriatal dopaminergic neurons, which is thought to underlie its motor symptoms such as resting tremor and dyskinesia. The loss of nigrostriatal dopamine is associated with loss of dendritic spines in the striatopallidal, but not striatonigral MSNs (Day et al., 2006). Despite the spine loss, the corticostriatal glutamatergic system could show increased activity after loss of dopaminergic input, resulting in neurophysiology coinciding with remodeling of axospinous synapses in the striatum (Calabresi et al., 1996; Marti et al., 1999).

In Villalba and Smith (2011), perfusion-fixed striatal tissue from parkinsonian monkeys treated with 1-methyl-4-phenyl-1,2,3,6-tetrahydropyridine (MPTP) was used to assess morphology of these synapses by ssEM. Immunoperoxidase staining for vesicular glutamate transporter (vGluT) 1 and vGluT2 differentiated dendritic spines receiving the cortical and (predominantly) thalamic inputs, respectively. Spines contacted by vGluT1-positive (cortical) boutons had larger volumes and larger PSDs than those contacted by vGluT2-

positive (thalamic) ones. A subset (5-10%) of vGluT2-positive boutons formed synapses with multiple postsynaptic structures (spines and dendritic shaft; Figs. 2G and G'), which was not the case with vGluT1-positive boutons. Thus, it appears that the cortical and thalamic afferents have different connectivity patterns and synaptic strengths with MSNs. MPTP treatment increased spine volume, size and perforation of PSD, and the volume of presynaptic boutons for both vGluT1 and vGluT2-expressing synapses. These ultrastructural changes associated with vGluT1-positive synapses are consistent with increased efficacy of corticostriatal pathway in parkinsonian conditions, while it remains to be established whether changes in vGluT2-expressing synapses are also correlated with altered neurophysiology. At corticostriatal synapses, MPTP treatment also increased the ratio of spine apparatus (SA) volume relative to the spine volume (Figs. 2H, H', I, and I'), as well as the number of mitochondria (which had smaller individual volumes) in the presynaptic boutons. Because they can span over dozens of serial ultrathin sections, methods other than ssEM would have overlooked these changes in the mitochondria and SA, which are implicated in metabolic state of presynaptic boutons, and the regulation of protein synthesis and Ca^{2+} in the spines, respectively (Fifkova et al., 1983; Pierce et al., 2000; Pierce et al., 2001; Rintoul et al., 2003; Verstreken et al., 2005; Tong, 2007).

The SA is composed of multiple cisterns of smooth endoplasmic reticulum with interdigitating dense plates (Gray, 1959; Spacek, 1985; Spacek and Harris, 1997; Cooney et al., 2002) and is enriched with the actin-binding protein synaptopodin (Deller et al., 2000; Deller et al., 2003; Deller et al., 2007). Only a subset of large spines in the normal forebrain contains the SA (Spacek, 1985; Spacek and Harris, 1997; Cooney et al., 2002), which is completely absent in mice lacking synaptopodin (Deller et al., 2003). In the human brain, previous observations in edematous and peritumorous tissue revealed abnormal SA morphology, including hypertrophy or hypotrophy as well as dilated cisterns of smooth endoplasmic reticulum (Fig. 3; Spacek, 1987; Castejon et al., 1995; Fiala et al., 2002). In some cases, dense plates of the SA appeared continuous with filamentous material that contacts the base of PSD (Fig. 3; also see Spacek, 1985; Spacek and Harris, 1997). These findings, along with Villalba and Smith (2011), suggest that pathological morphology of this organelle may indicate altered functional states of the associated spine synapses, and the SA functions may be compromised in multiple brain disorders and injuries. As mechanisms regulating the SA morphology become better characterized, the future ssEM analyses of this organelle may be able to extend our knowledge further by establishing correlations between disease pathology and specific changes in the SA ultrastructure (e.g., distribution along dendrites, and/or volume and complexity of the cisterns).

The data analysis by Villalba and Smith (2011) was limited to sampled spines contacted by immunolabeled boutons because only the superficial part of the tissue (where immunolabeling was optimal) could be used to disambiguate the two afferent populations. This study demonstrates an effective use of ssEM in combination with immunoperoxidase staining to examine afferent-specific remodeling of synapses in pathological conditions.

4. Concluding remarks

Aided by advanced molecular genetic tools and fluorescence-based light microscopy methods, the last decade saw a substantial gain in our understanding of molecular signaling mechanisms in which genes associated with susceptibility to various brain disorders affect the morphology and functions of dendritic spines. These studies may perhaps lead to identification of common molecular signaling pathways responsible for dendritic spine pathology, and could be exploited to develop novel therapeutic targets. However, because spines are the main sites of excitatory synapses in spiny neurons, pathological changes in spine morphology are often only part of the larger neuropathological processes involved in

the disruption of synaptic functions and circuitry architecture. The light microscopic findings need to be extended with ssEM analyses to examine changes in dendritic spines in the context of the broader neuronal circuitry, involving presynaptic partners and relationships with glial cells. Combined with immunolabeling methods, ssEM can be used to determine circuit-specific changes in synapse structures as well as 3D distribution of otherwise invisible molecules in relation to neuropil. The use of ssEM analyses on brain tissue from *in vivo* functional imaging studies presents an excellent opportunity to correlate ultrastructural changes at synapses with functional consequences during pathology. In addition, detailed ultrastructural analysis of organelles and other subcellular components also reveals invaluable clues regarding the cell biological mechanisms that underlie altered structure and functional states of individual synapses. For example, the spine apparatus (SA) appears to be involved in multiple brain pathologies (see above; Figs. 2H, 2I, and 3), and studies of this highly complex organelle would particularly benefit from ssEM analysis. The serial EM approach is required to ascertain its morphology and distribution because the SA can span the entire length of the associated spine (Fig. 2I'), and only a subset of large spines contains this organelle. Because it is involved in protein synthesis and Ca^{2+} regulation in the spines, pathological changes in the SA structure and distribution may indicate aberrant functional states of the associated spines and synapses, which may underlie disease pathology and/or symptoms.

The six studies featured above demonstrate advantages of ssEM analyses in a variety of brain disorders and systems. In the last decade, renewed interest in the use of ssEM has led to significant technological improvements of this high-resolution 3D tool. With ongoing development of better computational tools for managing and analyzing large stacks of serial EM images, ssEM analyses could become more routine. The insights gained from ssEM studies will help to elucidate the ultrastructural changes in synapses and connectivity, and ultimately targets for treating altered network activity and clinical symptoms.

Acknowledgments

We thank Patrick Parker for help in preparing the manuscript. This work was supported by grants from the National Institutes of Health (NS021184 and EB002170 to K.M.H.) and the Texas Emerging Technology Fund.

Abbreviations

3D	three-dimensional
Aβ	amyloid β
AD	Alzheimer's disease
ATLUM	automatic tape-collecting lathe ultramicrotome
CCD	charge-coupled device
DNMS	delayed nonmatching-to-sample
DS	Down's syndrome
EM	electron microscopy
FIB-SEM	focused ion beam-SEM
GABA	γ-aminobutylic acid
MPTP	1-methyl-4-phenyl-1,2,3,6-tetrahydropyridine
MSB	multi-synaptic bouton

MSNs	medium spiny neurons
MTLE	mesial temporal lobe epilepsy
NSB	non-synaptic bouton
PSD	postsynaptic density
SA	spine apparatus
SBFSEM	serial block face SEM
SEM	scanning electron microscopy
ssEM	serial section electron microscopy
STEM	scanning transmission electron microscopy
TEM	transmission electron microscopy
TEMCA	TEM camera array
vGluT	vesicular glutamate transporter

Reference List

Alonso-Nanclares L, Gonzalez-Soriano J, Rodriguez JR, DeFelipe J. Gender differences in human cortical synaptic density. Proc Natl Acad Sci U S A. 2008; 105:14615–14619. [PubMed: 18779570]

Anderson JR, Jones BW, Watt CB, Shaw MV, Yang JH, Demill D, Lauritzen JS, Lin Y, Rapp KD, Mastronarde D, Koshevoy P, Grimm B, Tasdizen T, Whitaker R, Marc RE. Exploring the retinal connectome. Mol Vis. 2011a; 17:355–79. 355-379. [PubMed: 21311605]

Anderson JR, Mohammed S, Grimm B, Jones BW, Koshevoy P, Tasdizen T, Whitaker R, Marc RE. The Viking viewer for connectomics: scalable multi-user annotation and summarization of large volume data sets. J Microsc. 2011b; 241:13–28. [PubMed: 21118201]

Blanpied TA, Ehlers MD. Microanatomy of dendritic spines: emerging principles of synaptic pathology in psychiatric and neurological disease. Biol Psychiatry. 2004; 55:1121–1127. [PubMed: 15184030]

Bock DD, Lee WCA, Kerlin AM, Andermann ML, Hood G, Wetzel AW, Yurgenson S, Soucy ER, Kim HS, Reid RC. Network anatomy and in vivo physiology of visual cortical neurons. Nature. 2011; 471:177–182. [PubMed: 21390124]

Bourne JN, Harris KM. Coordination of size and number of excitatory and inhibitory synapses results in a balanced structural plasticity along mature hippocampal CA1 dendrites during LTP. Hippocampus. 2011a; 21:354–373. [PubMed: 20101601]

Bourne JN, Harris KM. Nanoscale analysis of structural synaptic plasticity. Curr Opin Neurobiol. 2011b doi: 10.1016/j.conb.2011.10.019.

Bourne JN, Kirov SA, Sorra KE, Harris KM. Warmer preparation of hippocampal slices prevents synapse proliferation that might obscure LTP-related structural plasticity. Neuropharmacology. 2007; 52:55–59. [PubMed: 16895730]

Boyer C, Schikorski T, Stevens CF. Comparison of hippocampal dendritic spines in culture and in brain. J Neurosci. 1998; 18:5294–5300. [PubMed: 9651212]

Briggman KL, Denk W. Towards neural circuit reconstruction with volume electron microscopy techniques. Curr Opin Neurobiol. 2006; 16:562–570. [PubMed: 16962767]

Briggman KL, Helmstaedter M, Denk W. Wiring specificity in the direction-selectivity circuit of the retina. Nature. 2011; 471:183–188. [PubMed: 21390125]

Calabresi P, Pisani A, Mercuri NB, Bernardi G. The corticostriatal projection: from synaptic plasticity to dysfunctions of the basal ganglia. Trends Neurosci. 1996; 19:19–24. [PubMed: 8787136]

Cantoni M, Genoud C, Hebert C, Knott G. Large volume, isotropic, 3D imaging of cell structure on the nanometer scale. Microsc Anal. 2010; 24:13–16.

Castejon OJ, Valero C, Diaz M. Synaptic degenerative changes in human traumatic brain edema. An electron microscopic study of cerebral cortical biopsies. J Neurosurg Sci. 1995; 39:47–65. [PubMed: 8568555]

Chen X, Winters CA, Reese TS. Life inside a thin Section: tomography. J Neurosci. 2008; 28:9321–9327. [PubMed: 18799665]

Chklovskii DB, Vitaladevuni S, Scheffer LK. Semi-automated reconstruction of neural circuits using electron microscopy. Curr Opin Neurobiol. 2010; 20:667–675. [PubMed: 20833533]

Cooney JR, Hurlburt JL, Selig DK, Harris KM, Fiala JC. Endosomal compartments serve multiple hippocampal dendritic spines from a widespread rather than a local store of recycling membrane. J Neurosci. 2002; 22:2215–2224. [PubMed: 11896161]

D'Andrea MR, Nagele RG, Wang HY, Peterson PA, Lee DH. Evidence that neurones accumulating amyloid can undergo lysis to form amyloid plaques in Alzheimer's disease. Histopathology. 2001; 38:120–134. [PubMed: 11207825]

Dailey ME, Smith SJ. The dynamics of dendritic structure in developing hippocampal slices. J Neurosci. 1996; 16:2983–2994. [PubMed: 8622128]

Davisson MT, Schmidt C, Reeves RH, Irving NG, Akeson EC, Harris BS, Bronson RT. Segmental trisomy as a mouse model for Down syndrome. Prog Clin Biol Res. 1993; 384:117–133. [PubMed: 8115398]

Day M, Wang Z, Ding J, An X, Ingham CA, Shering AF, Wokosin D, Ilijic E, Sun Z, Sampson AR, Mugnaini E, Deutch AY, Sesack SR, Arbuthnott GW, Surmeier DJ. Selective elimination of glutamatergic synapses on striatopallidal neurons in Parkinson disease models. Nat Neurosci. 2006; 9:251–259. [PubMed: 16415865]

DeFelipe J. From the connectome to the synaptome: an epic love story. Science. 2010; 330:1198–1201. [PubMed: 21109663]

Pozueta J, Lefort R, Shelanski M. Synaptic changes in Alzheimer's disease and its models. Neuroscience. 2012 in press.

DeKosky ST, Scheff SW. Synapse loss in frontal cortex biopsies in Alzheimer's disease: correlation with cognitive severity. Ann Neurol. 1990; 27:457–464. [PubMed: 2360787]

Deller T, Bas Orth, C Del, Turco D, Vlachos A, Burbach GJ, Drakew A, Chabanis S, Korte M, Schwegler H, Haas CA, Frotscher M. A role for synaptopodin and the spine apparatus in hippocampal synaptic plasticity. Ann Anat. 2007; 189:5–16. [PubMed: 17319604]

Deller T, Korte M, Chabanis S, Drakew A, Schwegler H, Stefani GG, Zuniga A, Schwarz K, Bonhoeffer T, Zeller R, Frotscher M, Mundel P. Synaptopodin-deficient mice lack a spine apparatus and show deficits in synaptic plasticity. Proc Natl Acad Sci U S A. 2003; 100:10494–10499. [PubMed: 12928494]

Deller T, Merten T, Roth SU, Mundel P, Frotscher M. Actin-associated protein synaptopodin in the rat hippocampal formation: localization in the spine neck and close association with the spine apparatus of principal neurons. J Comp Neurol. 2000; 418:164–181. [PubMed: 10701442]

Demas GE, Nelson RJ, Krueger BK, Yarowsky PJ. Spatial memory deficits in segmental trisomic Ts65Dn mice. Behav Brain Res. 1996; 82:85–92. [PubMed: 9021073]

Denk W, Horstmann H. Serial block-face scanning electron microscopy to reconstruct three-dimensional tissue nanostructure. PLoS Biol. 2004; 2:e329. doi:10.1371/journal.pbio.0020329. [PubMed: 15514700]

Licznerski P, Duman RS. Remodeling of spine synapses in the pathophysiology and treatment of depression. Neuroscience. 2012 in press.

Feinberg, MD.; Szumowski, KM.; Harris, KM. Microwave fixation of rat hippocampal slices. In: Giberson, RT.; DeMaree, RSJ., editors. Microwave Techniques and Protocols. Humana Press; Totowa, New Jersey: 2001. p. 75-88.

Fiala JC. Reconstruct: a free editor for serial section microscopy. J Microsc. 2005; 218:52–61. [PubMed: 15817063]

Fiala JC, Feinberg M, Peters A, Barbas H. Mitochondrial degeneration in dystrophic neurites of senile plaques may lead to extracellular deposition of fine filaments. Brain Struct Funct. 2007; 212:195–207. [PubMed: 17717688]

Fiala JC, Feinberg M, Popov V, Harris KM. Synaptogenesis via dendritic filopodia in developing hippocampal area CA1. J Neurosci. 1998; 18:8900–8911. [PubMed: 9786995]

Fiala JC, Harris KM. Cylindrical diameters method for calibrating section thickness in serial electron microscopy. J Microsc. 2001a; 202:468–472. [PubMed: 11422668]

Fiala JC, Harris KM. Extending unbiased stereology of brain ultrastructure to three-dimensional volumes. J Am Med Inform Assoc. 2001b; 8:1–16. [PubMed: 11141509]

Fiala JC, Kirov SA, Feinberg MD, Petrak LJ, George P, Goddard CA, Harris KM. Timing of neuronal and glial ultrastructure disruption during brain slice preparation and recovery in vitro. J Comp Neurol. 2003; 465:90–103. [PubMed: 12926018]

Fiala JC, Spacek J, Harris KM. Dendritic spine pathology: cause or consequence of neurological disorders? Brain Res Rev. 2002; 39:29–54. [PubMed: 12086707]

Fifkova E, Markham JA, Delay RJ. Calcium in the spine apparatus of dendritic spines in the dentate molecular layer. Brain Res. 1983; 266:163–168. [PubMed: 6189559]

Frost NA, Kerr JM, Lu HE, Blanpied TA. A network of networks: cytoskeletal control of compartmentalized function within dendritic spines. Curr Opin Neurobiol. 2010; 20:578–587. [PubMed: 20667710]

Garcia O, Torres M, Helguera P, Coskun P, Busciglio J. A role for thrombospondin-1 deficits in astrocyte-mediated spine and synaptic pathology in Down's syndrome. PLoS One. 2010; 5:e14200. doi:10.1371/journal.pone.0014200. [PubMed: 21152035]

Glausier JR, Lewis DA, et al. Dendritic Spine Pathology in Schizophrenia. Neuroscience. 2012 in press.

Gouras GK, Tsai J, Naslund J, Vincent B, Edgar M, Checler F, Greenfield JP, Haroutunian V, Buxbaum JD, Xu H, Greengard P, Relkin NR. Intraneuronal Abeta42 accumulation in human brain. Am J Pathol. 2000; 156:15–20. [PubMed: 10623648]

Graveland GA, Williams RS, DiFiglia M. Evidence for degenerative and regenerative changes in neostriatal spiny neurons in huntington's disease. Science. 1985; 227:770–773. [PubMed: 3155875]

Gray EG. Electron microscopy of synaptic contacts on dendrite spines of the cerebral cortex. Nature. 1959; 183:1592–1593. [PubMed: 13666826]

Hanson JE, Blank M, Valenzuela RA, Garner CC, Madison DV. The functional nature of synaptic circuitry is altered in area CA3 of the hippocampus in a mouse model of Down's syndrome. J Physiol. 2007; 579:53–67. [PubMed: 17158177]

Hara Y, Park CS, Janssen WGM, Punsoni M, Rapp PR, Morrison JH. Synaptic characteristics of dentate gyrus axonal boutons and their relationships with aging, menopause, and memory in female rhesus monkeys. J Neurosci. 2011; 31:7737–7744. [PubMed: 21613486]

Hara Y, Park CS, Janssen WGM, Roberts MT, Morrison JH, Rapp PR. Synaptic correlates of memory and menopause in the hippocampal dentate gyrus in rhesus monkeys. Neurobiol Aging. 2012; 33:421.e17–421.e28. [PubMed: 21030115]

Harris, KM. Serial electron microscopy as an alternative or complement to confocal microscopy for the study of synapses and dendritic spines in the central nervous system. In: Stevens, JK.; Mills, LR.; Trogadis, JE., editors. Three-dimensional confocal microscopy: volume investigation of biological specimens. Academic Press; New York: 1994. p. 421-445.

Harris, KM.; Bourne, JN.; Mendenhall, JM.; Spacek, J. Hippocampal CA1 dendrites of greater caliber have more spines and contain more microtubules as a subcellular supply route; Program No. 147.19. 2007 Neuroscience Meeting Planner; San Diego, CA: Society for Neuroscience. 2007; Online

Harris KM, Kater SB. Dendritic Spines: Cellular Specializations Imparting Both Stability and Flexibility to Synaptic Function. Ann Rev Neurosci. 1994; 17:341–371. [PubMed: 8210179]

Harris KM, Perry E, Bourne J, Feinberg M, Ostroff L, Hurlburt J. Uniform serial sectioning for transmission electron microscopy. J Neurosci. 2006; 26

Harris KM, Stevens JK. Dendritic spines of rat cerebellar Purkinje cells: serial electron microscopy with reference to their biophysical characteristics. J Neurosci. 1988; 8:4455–4469. [PubMed: 3199186]

Harris KM, Stevens JK. Dendritic spines of CA 1 pyramidal cells in the rat hippocampus: serial electron microscopy with reference to their biophysical characteristics. J Neurosci. 1989; 9:2982–2997. [PubMed: 2769375]

Harris KM, Sultan P. Variation in the number, location and size of synaptic vesicles provides an anatomical basis for the nonuniform probability of release at hippocampal CA1 synapses. Neuropharmacology. 1995; 34:1387–1395. [PubMed: 8606788]

Harris, KM.; Weinberg, RJ. Ultrastructure of synapses in the mammalian brain. In: Sheng, M.; Sabatini, B.; Sudhof, TC., editors. The synapse. Cold Spring Harbor Perspectives in Biology; 2012. doi:10.1101/cshperspect.a005587

Hayat, MA. Fixation for electron microscopy. Academic Press; New York: 1981.

Hayworth KJ, Kasthuri N, Schalek R, Lichtman JW. Automating the collection of ultrathin serial sections for large volume TEM reconstructions. Microsc Microanal. 2006; 12:86–87.

He CX, Portera-Calliau C. The trouble with spines in Fragile X syndrome. Neuroscience. 2012 in press.

Helmstaedter M, Briggman KL, Denk W. 3D structural imaging of the brain with photons and electrons. Curr Opin Neurobiol. 2008; 18:633–641. [PubMed: 19361979]

Helmstaedter M, Briggman KL, Denk W. High-accuracy neurite reconstruction for high-throughput neuroanatomy. Nat Neurosci. 2011; 14:1081–1088. [PubMed: 21743472]

Henkemeyer M, Itkis OS, Ngo M, Hickmott PW, Ethell IM. Multiple EphB receptor tyrosine kinases shape dendritic spines in the hippocampus. J Cell Biol. 2003; 163:1313–1326. [PubMed: 14691139]

Hof PR, et al. Dendritic Spine Pathology in Aging. Neuroscience. 2012 in press.

Holtmaat A, Svoboda K. Experience-dependent structural synaptic plasticity in he mammalian brain. Nat Rev Neurosci. 2009; 10:647–658. [PubMed: 19693029]

Huang B, Bates M, Zhuang X. Super-resolution fluorescence microscopy. Ann Rev Biochem. 2009; 78:993–1016. [PubMed: 19489737]

Huotari J, Helenius A. Endosome maturation. EMBO J. 2011; 30:3481–3500. [PubMed: 21878991]

Hyde LA, Frisone DF, Crnic LS. Ts65Dn mice, a model for Down syndrome, have deficits in context discrimination learning suggesting impaired hippocampal function. Behav Brain Res. 2001; 118:53–60. [PubMed: 11163633]

Jain V, Seung HS, Turaga SC. Machines that learn to segment images: a crucial technology for connectomics. Curr Opin Neurobiol. 2010; 20:653–666. [PubMed: 20801638]

Kimura N, Yanagisawa K, Terao K, Ono F, Sakakibara I, Ishii Y, Kyuwa S, Yoshikawa Y. Age-related changes of intracellular Abeta in cynomolgus monkey brains. Neuropathol Appl Neurobiol. 2005; 31:170–180. [PubMed: 15771710]

Kimura N, Tanemura K, Nakamura S, Takashima A, Ono F, Sakakibara I, Ishii Y, Kyuwa S, Yoshikawa Y. Age-related changes of Alzheimer's disease-associated proteins in cynomolgus monkey brains. Biochem Biophys Res Commun. 2003; 310:303–311. [PubMed: 14521910]

Kirov SA, Petrak LJ, Fiala JC, Harris KM. Dendritic spines disappear with chilling but proliferate excessively upon rewarming of mature hippocampus. Neuroscience. 2004; 127:69–80. [PubMed: 15219670]

Kleinfeld D, Bharioke A, Blinder P, Bock DD, Briggman KL, Chklovskii DB, Denk W, Helmstaedter M, Kaufhold JP, Lee WCA, Meyer HS, Micheva KD, Oberlaender M, Prohaska S, Reid RC, Smith SJ, Takemura S, Tsai PS, Sakmann B. Large-scale automated histology in the pursuit of connectomes. J Neurosci. 2011; 31:16125–16138. [PubMed: 22072665]

Knott G, Rosset S, Cantoni M. Focussed ion beam milling and scanning electron microscopy of brain tissue. J Vis Exp. 2011; 2588 doi: 10.3791/2588.

Knott G, Holtmaat A. Dendritic spine plasticity Current understanding from in vivo studies. Brain Res Rev. 2008; 58:282–289. [PubMed: 18353441]

Knott GW, Holtmaat A, Wilbrecht L, Welker E, Svoboda K. Spine growth precedes synapse formation in the adult neocortex in vivo. Nat Neurosci. 2006; 9:1117–1124. [PubMed: 16892056]

Knowles-Barley S, Butcher NJ, Meinertzhagen IA, Armstrong JD. Biologically inspired EM image alignment and neural reconstruction. Bioinformatics. 2011; 27:2216–2223. [PubMed: 21742636]

Kubota Y, Hatada S, Kawaguchi Y. Important factors for the three-dimensional reconstruction of neuronal structures from serial ultrathin sections. Front Neural Circuits. 2009; 3:4. doi:10.3389/neuro.04.004.2009. [PubMed: 19521546]

Kurt MA, Kafa MI, Dierssen M, Davies DC. Deficits of neuronal density in CA1 and synaptic density in the dentate gyrus, CA3 and CA1, in a mouse model of Down syndrome. Brain Res. 2004; 1022:101–109. [PubMed: 15353219]

Kuwajima, M.; Mendenhall, JM.; Harris, KM. Large-volume reconstruction of brain tissue from high-resolution serial section images acquired by SEM-based scanning transmission electron microscopy. In: Sousa, AA.; Kruhlak, MJ., editors. Methods in Molecular Biology – Nanoimaging: Methods and Protocols. Humana Press; 2012. in press

Lacor PN, Buniel MC, Furlow PW, Sanz Clemente A, Velasco PT, Wood M, Viola KL, Klein WL. A(beta) oligomer-induced aberrations in synapse composition, shape, and density provide a molecular basis for loss of connectivity in Alzheimer's disease. J Neurosci. 2007; 27:796–807. [PubMed: 17251419]

Lang S, Drouvelis P, Tafaj E, Bastian P, Sakmann B. Fast extraction of neuron morphologies from large-scale SBFSEM image stacks. J Comput Neurosci. 2011; 31:533–545. [PubMed: 21424815]

Leuner B, Shors TJ. Stress, anxiety, and dendritic spines: What are the connections? Neuroscience. 2012 in press.

Lichtman JW, Denk W. The big and the small: challenges of imaging the brain's circuits. Science. 2011; 334:618–623. [PubMed: 22053041]

Lisman JE, Harris KM. Quantal analysis and synaptic anatomy – integrating two views of hippocampal plasticity. Trends Neurosci. 1993; 16:141–147. [PubMed: 7682347]

Mancuso JJ, Yuanxin C, Xuping L, Wong STC. Methods of dendritic spine detection: from Golgi to high resolution optical imaging. Neuroscience. 2012 in press.

Marti M, Sbrenna S, Fuxe K, Bianchi C, Beani L, Morari M. In vitro evidence for increased facilitation of striatal acetylcholine release via pre- and postsynaptic NMDA receptotors in hemiparkinsonian rats. J Neurochem. 1999; 72:875–878. [PubMed: 9930765]

Martin LJ, Sisodia SS, Koo EH, Cork LC, Dellovade TL, Weidemann A, Beyreuther K, Masters C, Price DL. Amyloid precursor protein in aged nonhuman primates. Proc Natl Acad Sci U S A. 1991; 88:1461–1465. [PubMed: 1899927]

Mateos JM, Luthi A, Savic N, Stierli B, Streit P, Gahwiler BH, McKinney RA. Synaptic modifications at the CA3 CA1 synapse after chronic AMPA receptor blockade in rat hippocampal slices. J Physiol. 2007; 581:129–138. [PubMed: 17303644]

Matus A. Actin-based plasticity in dendritic spines. Science. 2000; 290:754–758. [PubMed: 11052932]

McDonald K. A review of high-pressure freezing preparation techniques for correlative light and electron microscopy of the same cells and tissues. J Microsc. 2009; 235:273–281. [PubMed: 19754722]

Mendenhall, JM.; Yorston, J.; Lagarec, KG.; Bowden, J.; Harris, KM. Large volume high resolution imaging of brain neuropil using SEM-based scanning electron microscpy; Program No. 484.17. 2009 Neuroscience Meeting Planner; Chicago, IL: Society for Neuroscience. 2009; Online

Micheva KD, Smith SJ. Array tomography: a new tool for imaging the molecular architecture and ultrastructure of neural circuits. Neuron. 2007; 55:25–36. [PubMed: 17610815]

Mishchenko Y, Hu T, Spacek J, Mendenhall J, Harris KM, Chklovskii DB. Ultrastructural analysis of hippocampal neuropil from the connectomics perspective. Neuron. 2010; 67:1009–1020. [PubMed: 20869597]

Morales J, Alonso-Nanclares L, Rodriguez JR, DeFelipe J, Rodriguez A, Merchan-Perez A. Espina: a tool for the automated segmentation and counting of synapses in large stacks of electron microscopy images. Front Neuroanat. 2011; 5:18. [PubMed: 21633491]

Nithianantharajah J, Hannan AJ. Dysregulation of synaptic proteins, dendritic spine abnormalities and pathological plasticity of synapses as mediators of cognitive and psychiatric symptoms in Huntington's disease. Neuroscience. 2012 in press.

Novikoff PM, Novikoff AB, Quintana N, Hauw JJ. Golgi apparatus, GERL, and lysosomes of neurons in rat dorsal root ganglia, studied by thick section and thin section cytochemistry. J Cell Biol. 1971; 50:859–886. [PubMed: 4329159]

Nuntagij P, Oddo S, LaFerla FM, Kotchabhakdi N, Ottersen OP, Torp R. Amyloid deposits show complexity and intimate spatial relationship with dendrosomatic plasma membranes: an electron microscopic 3D reconstruction analysis in 3xTg-AD mice and aged canines. J Alzheimers Dis. 2009; 16:315–323. [PubMed: 19221421]

Oddo S, Caccamo A, Shepherd JD, Murphy MP, Golde TE, Kayed R, Metherate R, Mattson MP, Akbari Y, LaFerla FM. Triple-transgenic model of Alzheimer's disease with plaques and tangles. Neuron. 2003; 39:409–421. [PubMed: 12895417]

Ohyagi Y. Intracellular amyloid beta-protein as a therapeutic target for treating Alzheimer's disease. Curr Alzheimer Res. 2008; 5:555–561. [PubMed: 19075582]

Ostroff LE, Fiala JC, Allwardt B, Harris KM. Polyribosomes redistribute from dendritic shafts into spines with enlarged synapses during LTP in developing rat hippocampal slices. Neuron. 2002; 35:535–545. [PubMed: 12165474]

Palay SL, Palade GE. The fine structure of neurons. J Biophys Biochem Cytol. 1955; 1:69–88. [PubMed: 14381429]

Penzes P, Cahill ME, Jones KA, VanLeeuwen JE, Woolfrey KM. Dendritic spine pathology in neuropsychiatric disorders. Nat Neurosci. 2011; 14:285–293. [PubMed: 21346746]

Peters A, Kaiserman-Abramof IR. The small pyramidal neuron of the rat cerebral cortex. The synapses upon dendritic spines. Z Zellforsch Mikrosk Anat. 1969; 100:487–506. [PubMed: 5351190]

Pierce JP, van Leyen K, McCarthy JB. Translocation machinery for synthesis of integral membrane and secretory proteins in dendritic spines. Nat Neurosci. 2000; 3:311–313. [PubMed: 10725917]

Pierce JP, Mayer T, McCarthy JB. Evidence for a satellite secretory pathway in neuronal dendritic spines. Curr Biol. 2001; 11:351–355. [PubMed: 11267872]

Popov VI, Kleschevnikov AM, Klimenko OA, Stewart MG, Belichenko PV. Three-dimensional synaptic ultrastructure in the dentate gyrus and hippocampal area CA3 in the Ts65Dn mouse model of down syndrome. J Comp Neurol. 2011; 519:1338–1354. [PubMed: 21452200]

Purpura DP. Dendritic spine "dysgenesis" and mental retardation. Science. 1974; 186:1126–1128. [PubMed: 4469701]

Cajal, S. Histology of the nervous system of man and vertebrates. Oxford University Press; New York: 1995. Translated by Swanson N, Swanson LW

Reeves RH, Irving NG, Moran TH, Wohn A, Kitt C, Sisodia SS, Schmidt C, Bronson RT, Davisson MT. A mouse model for Down syndrome exhibits learning and behaviour deficits. Nat Genet. 1995; 11:177–184. [PubMed: 7550346]

Rintoul GL, Filiano AJ, Brocard JB, Kress GJ, Reynolds IJ. Glutamate decreases mitochondrial size and movement in primary forebrain neurons. J Neurosci. 2003; 23:7881–7888. [PubMed: 12944518]

Roelandse M, Matus A. Hypothermia-associated loss of dendritic spines. J Neurosci. 2004; 24:7843–7847. [PubMed: 15356196]

Roizen NJ, Patterson D. Down's syndrome. Lancet. 2003; 361:1281–1289. [PubMed: 12699967]

Russo SJ, Dietz DM, Dumitriu D, Morrison JH, Malenka RC, Nestler EJ. The addicted synapse: mechanisms of synaptic and structural plasticity in nucleus accumbens. Trends Neurosci. 2010; 33:267–276. [PubMed: 20207024]

Saalfeld S, Cardona A, Hartenstein V, Tomancak P. As-rigid-as-possible mosaicking and serial section registration of large ssTEM datasets. Bioinformatics. 2010; 26:i57–i63. [PubMed: 20529937]

Shankar GM, Bloodgood BL, Townsend M, Walsh DM, Selkoe DJ, Sabatini BL. Natural oligomers of the Alzheimer amyloid-(beta) protein induce reversible synapse loss by modulating an NMDA-type glutamate receptor-dependent signaling pathway. J Neurosci. 2007; 27:2866–2875. [PubMed: 17360908]

Sheng M, Hoogenraad CC. The postsynaptic architecture of excitatory synapses: a more quantitative view. Ann Rev Biochem. 2007; 76:823–847. [PubMed: 17243894]

Shepherd GMG, Harris KM. Three-Dimensional Structure and Composition of CA3→ CA1 Axons in Rat Hippocampal Slices: Implications for Presynaptic Connectivity and Compartmentalization. J Neurosci. 1998; 18:8300–8310. [PubMed: 9763474]

Smith Y, Bevan MD, Shink E, Bolam JP. Microcircuitry of the direct and indirect pathways of the basal ganglia. Neuroscience. 1998; 86:353–387. [PubMed: 9881853]

Smith Y, Raju D, Nanda B, Pare JF, Galvan A, Wichmann T. The thalamostriatal systems: Anatomical and functional organization in normal and parkinsonian states. Brain Res Bull. 2009; 78:60–68. [PubMed: 18805468]

Sorra KE, Harris KM. Occurrence and Three-Dimensional Structure of Multiple Synapses Between Individual Radiatum Axons and Their Target Pyramidal Cells in Hippocampal Area CA1. J Neurosci. 1993; 13:3736–3748. [PubMed: 8366344]

Spacek J. Ultrastructural pathology of dendritic spines in epitumorous human cerebral cortex. Acta Neuropathol. 1987; 73:77–85. [PubMed: 3604575]

Spacek J, Harris KM. Three-dimensional organization of smooth endoplasmic reticulum in hippocampal CA1 dendrites and dendritic spines of the immature and mature rat. J Neurosci. 1997; 17:190–203. [PubMed: 8987748]

Spacek J, Lieberman AR. Ultrastructure and three-dimensional organization of synaptic glomeruli in rat somatosensory thalamus. J Anat. 1974; 117:487–516. [PubMed: 4370696]

Spacek J. Three-dimensional analysis of dendritic spines. Anat Embryol. 1985; 171:235–243. [PubMed: 3985372]

Spencer SS. When should temporal-lobe epilepsy be treated surgically? Lancet Neurol. 2002; 1:375–382. [PubMed: 12849399]

Stevens JK, Davis TL, Friedman N, Sterling P. A systematic approach to reconstructing microcircuitry by electron microscopy of serial sections. Brain Res. 1980; 2:265–293. [PubMed: 6258704]

Studer D, Humbel BM, Chiquet M. Electron microscopy of high pressure frozen samples: bridging the gap between cellular ultrastructure and atomic resolution. Histochem Cell Biol. 2008; 130:877–889. [PubMed: 18795316]

Swann JW, Al Noori S, Jiang M, Lee CL. Spine loss and other dendritic abnormalities in epilepsy. Hippocampus. 2000; 10:617–625. [PubMed: 11075833]

Tao-Cheng JH, Gallant PE, Brightman MW, Dosemeci A, Reese TS. Structural changes at synapses after delayed perfusion fixation in different regions of the mouse brain. J Comp Neurol. 2007; 501:731–740. [PubMed: 17299754]

Thaemert JC. Ultrastructural interrelationships of nerve processes and smooth muscle cells in three dimensions. J Cell Biol. 1966; 28:37–49. [PubMed: 5322460]

Tong JJ. Mitochondrial delivery is essential for synaptic potentiation. Biol Bull. 2007; 212:169–175. [PubMed: 17438209]

Verstreken P, Ly CV, Venken KJT, Koh TW, Zhou Y, Bellen HJ. Synaptic mitochondria are critical for mobilization of reserve pool vesicles at Drosophila neuromuscular junctions. Neuron. 2005; 47:365–378. [PubMed: 16055061]

Villalba RM, Smith Y. Dendritic spine pathology in Parkinson's Disease and Drug Addiction: Is Striatal Dopaminergic Dysfunction the Common Target? Neuroscience. 2012 in press.

Villalba RM, Smith Y. Differential structural plasticity of corticostriatal and thalamostriatal axo-spinous synapses in MPTP-treated parkinsonian monkeys. J Comp Neurol. 2011; 519:989–1005. [PubMed: 21280048]

Witcher MR, Kirov SA, Harris KM. Plasticity of perisynaptic astroglia during synaptogenesis in the mature rat hippocampus. Glia. 2007; 55:13–23. [PubMed: 17001633]

Witcher MR, Park YD, Lee MR, Sharma S, Harris KM, Kirov SA. Three dimensional relationships between perisynaptic astroglia and human hippocampal synapses. Glia. 2010; 58:572–587. [PubMed: 19908288]

Wong M, Guo D. Dendritic spine pathology in epilepsy: Cause or consequence? Neuroscience. 2012 in press.

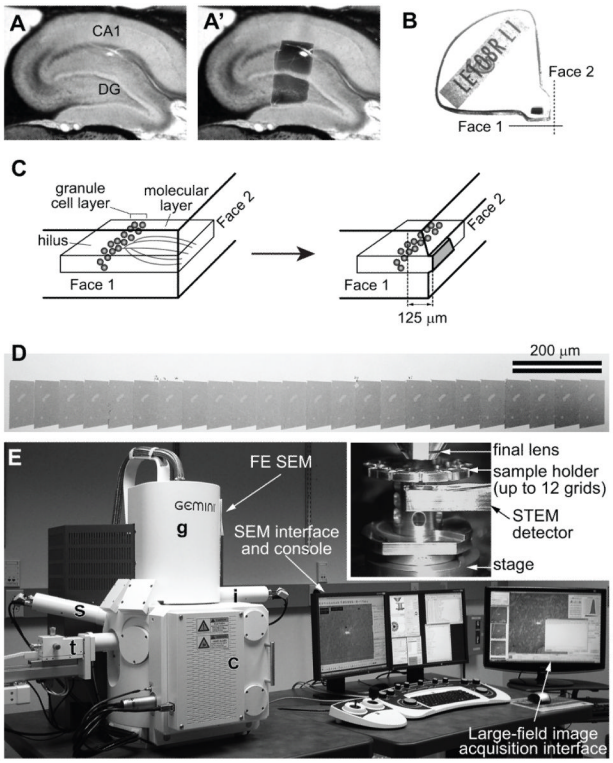

Figure 1.

An example of the rat hippocampal dentate gyrus tissue embedded into a “Chien mold” block for accurate targeting of the region of interest for serial EM imaging. (Figures from Kuwajima et al., 2012)

A: A parasagittal slice (70 μm thickness) of the hippocampal formation from a perfusionfixed rat. Area CA1 and the dentate gyrus (DG) are indicated.

A’: The same slice as in A, with a superimposed image of the dentate tissue embedded in the epoxy block shown in B.

B: The “Chien mold” was used to embed the dentate tissue dissected from the slice shown in A and A’ into epoxy resin. Note that the tissue can be cut from two faces of the block (Faces 1 and 2). A paper label identifying the block (“LE108RL1”) was embedded into resin along with the tissue.

C: *Left* – A diagram indicating the orientation of the tissue in the block shown in B. The “Face 1” is perpendicular to the granule cell layer (gray spheres) and the “Face 2”, and dendrites of these cells (gray curved lines in the molecular layer) are cut longitudinally in this plane. Test-thin sections taken from Face 1 are used to measure the distance from the cell layer. The “Face 2” is parallel to the cell layer, and therefore the dendrites are cut in cross-sections. *Right* – The same block after trimming the final block face (gray trapezoid area) for serial sectioning. In this example, serial sections are cut from the Face 2 at 125 μm from the top of the granule cell layer to target the middle molecular layer.

D: A low-magnification SEM image of a segment of serial sections on a single Pioloformcoated grid. Large capillaries are evident in each section.

E: For serial EM imaging, our laboratory uses a field emission scanning EM (FE SEM) that is equipped with a secondary electron detector (s), an in-lens detector (i), and a retractable detector for transmitted electrons (STEM detector; t). The column (g) contains the gun assembly and objective lenses. The specimen chamber door (c) slides open outward with the stage. The SEM is controlled through the SEM interface and console (keyboard and joysticks can be seen in front of the monitors), or the integrated large-field image acquisition

interface. *Inset* – TV camera view of the specimen chamber showing the arrangement of the final lens, STEM detector, and sample holder clipped onto the stage. The distance between the final lens and the specimen is 4-5 mm.

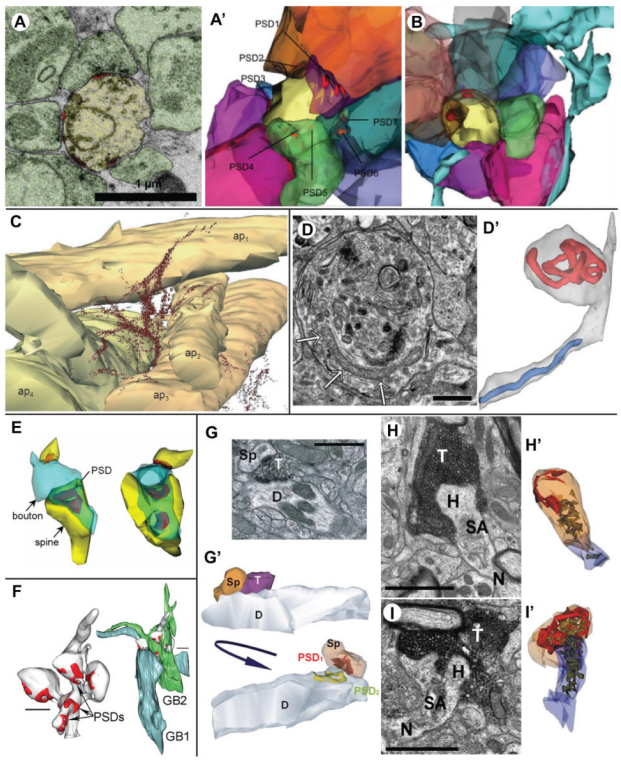

Figure 2.

A and B: Multisynaptic spines in the severe case of mesial temporal lobe epilepsy. A – Electron micrograph of a multisynaptic spine (yellow) with four synapses (red) and seven axons (green) that eventually synapse with this spine visible on this one section. A' – 3D reconstruction of the same multisynaptic spine (yellow) showing all nine of its presynaptic axonal boutons (multicolored) and seven of its PSDs (eight and nine are hidden). B – In the severe case, the astroglial processes (turquoise) were loosely associated around the periphery of many presynaptic axons (multicolored) making synapses on a single multisynaptic spine (yellow). From Witcher et al. (2010).

C: 3D reconstruction of extracellular deposits of amyloid β (Aβ) in the hippocampal stratum radiatum of a transgenic mouse model of Alzheimer's disease. Aβ deposits (dots representing gold particles) form continuous bundles of fibrils varying in size and direction, some of which are associated with apical dendrites (ap1-ap4). The reconstruction was made from ~100 serial sections with post-embedding immunogold labeling for Aβ. Scale bar = 0.5 μm. Reprinted from Journal of Alzheimer's Disease, Nuntagij P et al. (2009), Copyright 2009, with permission from IOS Press.

D: Electron micrograph of a neurite diverticulum, containing a long, curved mitochondrion (arrows) located adjacent to a curved microtubule. D' – 3D reconstruction of mitochondria in the same neurite demonstrates that the mitochondrion in the main axis (blue) has a normal cylindrical shape while the mitochondrion in the diverticulum (red) is convoluted and branching. Scale bar = 0.5 μm. Figures were reprinted from Fiala et al. (2007), Copyright 2007, with permission from Springer (pending).

E: 3D reconstruction of multi-synaptic boutons (MSB; blue) with the spines (yellow) and PSDs (red) in the outer molecular layer of the monkey hippocampal dentate gyrus. Both MSBs form a synapse with one small spine with macular PSD, and another with a large mushroom spine with perforated PSD. Perforated PSD can be in a single piece with perforation (left), or completely segmented (right). Reprinted from The Journal of

Neuroscience, Hara et al. (2011), Copyright 2011, with permission from the Society for Neuroscience.

F: Representative 3D reconstructions of two giant mossy fiber boutons (GB; green and blue) contacting a thorny excrescence (gray) with multiple PSDs (red) in the mouse hippocampal area CA3. Scale bar = 1 μm. Reprinted from The Journal of Comparative Neurology, Popov et al. (2011), Copyright 2011, with permission from John Wiley & Sons.

G-I: Afferent specific changes in axospinous synapses in the striatum of parkinsonian monkeys. G – Electron micrograph of a vGluT2-positive bouton (T) forming synapses with a dendritic shaft (D) and a spine (Sp). G' – 3D reconstruction of the same synapses, viewed from two angles, illustrating the spatial relationship of the bouton (T) with its postsynaptic partners (D and Sp), as well as the synapses (PSD1 and PSD2) that are perforated. H and I – Electron micrographs (H and I) and 3D reconstructions (H' and I') of representative axospinous synapses receiving inputs from vGluT1-positive boutons (T) in control (H and H') and parkinsonian (I and I') animals. The reconstructions illustrate the spatial arrangements of the spine apparatus (SA; green) and PSD (red) in the spine head (H) and neck (N). Scale bar = 1 μm in E, F, and G. Reprinted from The Journal of Comparative Neurology, Villalba and Smith (2011), Copyright 2011, with permission from John Wiley & Sons.

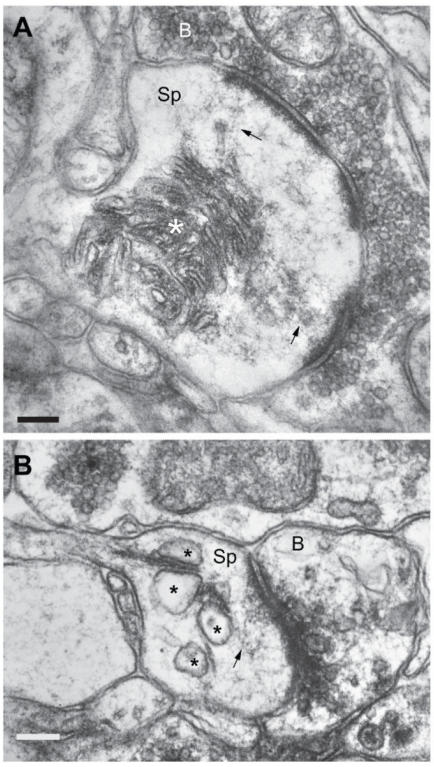

Figure 3.
A and B: Electron micrographs demonstrating changes in the spine apparatus morphology in peritumorous neocortical tissue from human patients. A – A large spine (Sp) forming a perforated asymmetric synapse with a bouton (B) contains a hypertrophic spine apparatus (asterisk). B – Another spine (Sp) containing a spine apparatus with dilated cisterns of smooth endoplasmic reticulum (asterisks). This spine forms an asymmetric synapse with a bouton (B) containing vesicles that appear to be disrupted. In both A and B, the dense plate of the spine apparatus appears to give rise to filamentous material (arrows) that contacts the base of PSD. Scale bars = 0.2 μm in A and B. Electron micrograph in A is from Spacek (1987).